Photochemical & Photobiological Sciences

PAPER

Cite this: *Photochem. Photobiol. Sci.*, 2016, **15**, 481

A ruthenium(II) based photosensitizer and transferrin complexes enhance photo-physical properties, cell uptake, and photodynamic therapy safety and efficacy

Pavel Kaspler,[a] Savo Lazic,[a] Sarah Forward,[b] Yaxal Arenas,[a] Arkady Mandel[a] and Lothar Lilge*[b]

Received 7th December 2015,
Accepted 23rd February 2016

DOI: 10.1039/c5pp00450k

www.rsc.org/pps

Metal-based photosensitizers are of interest as their absorption and chemical binding properties can be modified *via* the use of different ligands. Ru^{2+} based photosensitizers are known to be effective photodynamic therapy (PDT) agents against bacteria, whereas use for oncological indications *in vivo* has not been demonstrated with the same level of evidence. We present data showing that premixing the Ru^{2+}-complex TLD1433 with transferrin increases the molar extinction coefficient, including longer activation wavelengths, reduces photobleaching rates, and reduces the toxicity of the complex improving overall PDT efficacy. As the transferrin receptor is upregulated in most malignancies, premixing the Ru^{2+} complex with transferrin converts the active pharmaceutical ingredient TLD1433 into a drug of potentially considerable clinical utility.

Introduction

Photodynamic therapy (PDT) is a potential alternative or supplement to conventional cancer treatment. PDT uses a photosensitizer (PS) at non-toxic concentrations.[1,2] The reactive excited state photosensitizer (PS*), produced following photon absorption, participates in electron transfer reactions with biomolecules (Type I) or energy transfer with molecular oxygen ($^3O_2$) forming reactive oxygen species (ROS) such as superoxide radical anions or singlet oxygen ($^1O_2$) (Type II).[3] ROS or electron transfer reactions destroy malignant tissue *via* direct cellular effects, as with aminolevulinic acid (ALA) derived protoporphyrin IX (PpIX),[4] or *via* vascular effects as for TOOKAD®,[5] benzoporphyrin derivative mono acid A, and mTHPC,[6,7] and predominantly with Photofrin®.[8]

PSs have been shown to preferentially accumulate in proliferating cells, providing selectivity at the cellular level. Specificity of cytotoxic damage is achieved by three mechanisms: the short ROS lifetime, preferential accumulation of the PS, and confinement of the photon density by light scattering. The $^1O_2$ and hydroxyl radical lifetime is ~200 ns *in vitro*[9] and *in vivo*,[10] confining ROS activity within 1 μm of the PS. The treatment volume can be confined by selecting position of photon sources inside it and to control the sources power and exposure time. Resistance to photobleaching, oxygen independent activity, and near-infrared activation are additional desirable photosensitizer properties to increase PDT efficacy.

The use of PDT in oncology is not widespread due to limitations of approved PSs. The cytotoxic effect elicited by porphyrin-based PSs[1,2] depends on $^3O_2$, precluding cell death in hypoxic tissue pockets. Organic PSs can suffer from limited water-solubility, prolonged retention in tissues and photobleaching. Porphyrin based photosensitizers in their native form have not been shown to exploit active cell uptake by overexpressed transmembrane transport, so inhibiting transmembrane exporters such as the ABCG2 transporter has been shown to increase the cellular concentration of PpIX.[11]

Selective accumulation of metal coordination complexes in malignant tumors *versus* normal host tissue is required for highly selective oncological applications. Cellular selectivity can be attained by high metabolic activity and limiting enzymatic activity[12,13] or utilizing delivery agents such as liposomes decorated with antibodies to the desired upregulated tumor cell surface marker as the endothelial growth factor receptor (EGFR)[14] or similarly constructed nanoparticles.[15] Alternatively, selective accumulation can be provided by exploiting upregulated surface receptors and transmembrane transporters in malignancies.

The benefits of Ru^{2+} complexes are their controllable design, preparation, isolation, purification, and a potentially

[a]*Theralase Inc., 1945 Queen Street East, Toronto, ON M4L1H7, Canada*
[b]*University Health Network, Princess Margaret Cancer Research Tower and University of Toronto, Department of Medical Biophysics, 101 College Street, Toronto, ON M5G1L7, Canada. E-mail: llilge@uhnres.utoronto.ca; Tel: +1(416)581-8642*

high $^1O_2$ quantum yield.[16] Additionally, it has been demonstrated that coordination complexes[17] may not require oxygen to exert a cytotoxic effect.[18–25] The pseudo-octahedral complexes provided by Ru^{2+} allow design options for ligands providing affinity for DNA binding,[26] overall stability, and solubility as seen for [Ru(2,2′-bipyridine)-2-benzo[*i*]dipyrido-[3,2-*a*:2′,3′-*c*]phenazine]$^{2+}$, which can act as Type I or II agents.[26] Cellular and nuclear uptake has been shown *in vitro* for Ru^{2+} polypyridyl complexes.[27] A detractor for these complexes is their high triplet state energy, which requires short wavelength excitation photons. For example, dyad-based ligands require photon energies >2.1 eV,[28,29] while phenanthroline-based ligands require >1.8–1.9 eV.[19]

To simplify drug development efforts, a standard approach is to exploit a natural association of the active pharmaceutical ingredient with serum proteins and associated upregulated transmembrane transporters in malignant tissues. Upon administration, Ru^{2+} complexes associate with albumin[30] and transferrin,[31] enabling receptor-mediated transport into cells. Collagen of the extracellular matrix and actin in the cell are potentially involved in the anti-metastatic action of Ru^{2+} complexes.[32]

The vast majority of cancers show an upregulation of the transferrin receptor (Tf-R) as malignant cells require to boost their Fe^{3+} stores. The expression of Tf-R correlates with tumor grade, stage, progression, and metastasis,[33,34] notably in bladder cancer.[35] Investigating the Tf-R as a photosensitizer transport mechanism was initiated by Cavanaugh *et al*. with the synthesis of a deliberate chlorine e6–Tf complex which however, resulted in reduced single oxygen yield, absorption in the Soret band, and ultimately a reduced PDT effect.[36] Similar approaches for Tf-R-mediated uptake include covalent binding of Tf to a hematoporphyrin derivative[37] and a Tf-decorated liposomal formulation for $AlClPc_4$ [35,38] and Foscan (mTHPC) delivery, whereby only $AlClPc_4$ had improved selectivity in a rat bladder cancer model.

Photo-physical and photo-biological effects due to Ru^{2+} association with Tf are not well understood. Here, we report the effects of Tf binding with the [Ru(II)(4,4′-dimethyl-2,2′-bipyridine(dmb))$_2$(2-(2′,2″:5″,2‴-terthiophene)-imidazo[4,5-*f*]-[1,10]phenanthroline)]$^{2+}$ complex known as TLD1433, see Fig. 1 for the structure. The TLD1433–Tf complex is referred to as Rutherrin. Previous studies have demonstrated that TLD1433 has some nuclear localization in cells *in vitro* and a high affinity for DNA isolates in solution. TLD1433 provides a strong excited state reduction potential of 1.31 eV and an oxidation potential of −0.87 eV. TLD1433 showed a high therapeutic index between dark- and light-mediated toxicity *in vitro*, with more than 1.5 logs of PDT-mediated cell kill which can be increased due to the high photostability of the photosensitizer permitting a trade-off between the drug and photons whereby the light mediated toxicity LD_{50} can be <1 nM for 532 nm radiant exposure (H) > 90 J cm^{-2}.[18] This study investigated the differences in the changes in absorption spectra, ROS production, and PDT efficacy *in vitro* and *in vivo* between TLD1433 and Rutherrin.

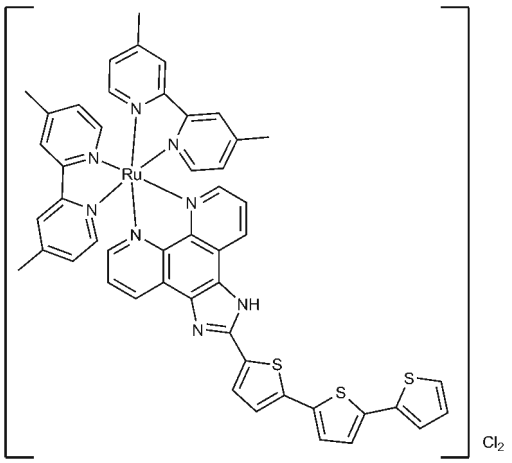

Fig. 1 Schematic of the [Ru(II)(4,4′-dimethyl-2,2′-bipyridine(dmb))$_2$-(2-(2′,2″:5″,2‴-terthiophene)-imidazo[4,5-*f*][1,10]phenanthroline)]$^{2+}$ complex known as TLD1433.

Materials and methods

Photosensitizer

The TLD1433 structure and synthesis have been described previously.[16,19,39,40] The stock (2 mM) was prepared in deionized water. TLD1433 was administered alone or following premixing with either human, murine, or bovine Tf with (holo-Tf) or without (apo-Tf) Fe^{2+} saturation. The letter m (murine) or b (bovine) preceding Rutherrin indicates the Tf species used if other than human Tf. Holo- as a second prefix indicates the use of holo-Tf in Rutherrin, otherwise it is apo-Tf. Tf concentrations were limited to 12.5 μM which is ~5 times the human concentration in serum.

Reagents

Singlet Oxygen Sensor Green (SOG, Cat# S36002), 3′-*p*-(hydroxyphenyl)fluorescein (HPF, Cat# H36004), NucBlue® Live nuclear dye (Cat# R37605), and Presto Blue reagent (Cat# A13261) were purchased from Life Technologies. *N*,*N*′-Dimethylthiourea (DMTU, Cat# D188700), bovine serum albumin (Cat# A-9418), sodium azide (NaN_3, Cat# 13412), HCl (Cat# 320331), bovine apo-transferrin (Cat# T1428), human apo-transferrin (Cat# T2036), human holo-transferrin (Cat# T0665) and mouse apo-transferrin (Cat# T0523) were purchased from Sigma-Aldrich.

Spectroscopic studies

Absorbance of 10 μM TLD1433 or Rutherrin was measured in quartz cuvettes in a dual beam spectrophotometer (Cary 300 Bio UV-Visible spectrophotometer, Varian Inc., FL07033947, CA). References were either deionized water, 10 mM phosphate buffer with 100 mM NaCl at pH = 7.2 (PBS), incomplete DMEM, or complete DMEM. Spectra were collected within 60 seconds of mixing the compounds. To detect a spectral signature associated with binding of TLD1433 to b-Tf, the spectra of both b-Tf and TLD1433 were subtracted from the b-Rutherrin spectrum. Similarly, signatures of binding to holo-Tf were obtained.

Luminescence, comprising fluorescence or phosphorescence, of 10 μM TLD1433 and b-Rutherrin in 10 mM PBS was measured following excitation at 380 or 470 nm, and detected from 520 to 800 nm using a dual grating fluorescence spectrofluorometer (Fluorolog, HORIBA Jobin Yvon, Edison, NJ, USA) in samples with absorbance of less than 0.2 per 3 mm path length at the excitation wavelength.

Transferrin and BSA binding kinetics and pH dependence

To determine the binding of TLD1433 to transferrin or BSA, 10 μM of the PS and protein were prepared in 10 mM phosphate buffered solution with 100 mM NaCl. Absorption spectroscopy as described above commenced immediately post mixing and continued for 20 minutes. For pH dependence measurements the pH was reduced using 3% or 1.5% HCl in multiple acidification steps from 7.38 to 3.17 followed at each step with spectroscopic analysis.

Photobleaching

Photobleaching of 10 μM TLD1433 or b-Rutherrin was determined in 10 mM PBS by exposing the solution to 525 nm photons (130 mW cm^{-2}) as a function of $H < 200$ J cm^{-2}, quantifying 432 nm absorbance.

ROS quantification

The ROS production of 500 μM TLD1433 or b-Rutherrin (2.5–10 μM b-Tf) was measured *via* fluorescent reporters: 100 μM SOG for $^1O_2$ and 100 μM HPF for the hydroxyl radical ($^{\bullet}HO$). To reveal non-specific signals, 100 mM DMTU and 10 mM sodium azide were used as $^{\bullet}HO$ and $^1O_2$ scavengers, respectively. 96-Well plates were irradiated with 625 nm light (119 mW cm^{-2}) for $H = 90$ J cm^{-2}. At predetermined times, irradiation was suspended and the fluorescence signals of SOG ($\lambda_{ex} = 494$ nm and $\lambda_{em} = 525$ nm) and HPF ($\lambda_{ex} = 490$ nm and $\lambda_{em} = 515$ nm) were obtained using a plate reader (SpectroMax plate reader, Molecular Devices, Sunnyvale, CA, US). The PDT-related ROS signal was determined by subtracting the SOG and HPF fluorescence in the presence of scavengers from the total signal of control samples. The ROS was measured using water, incomplete DMEM (without FBS and antibiotics) and complete DMEM (supplemented with FBS and antibiotics) as solvents.

Cell culture

Human (HT1376, ATCC #CRL-1472) and rat (AY27, a gift from Dr Selman at the University of Toledo, Toledo, OH) bladder carcinoma were used in *in vitro* experiments. Bladder cancer just like other malignancies shows an upregulation of the Tf-R. Here bladder cancer cell lines were selected as representatives of the first indication for clinical trials of TLD1433 mediated PDT. H1376 cells were confirmed *via* short tandem repeat profiles, which were not available for AY27 cells. Cells were cultured either in RPMI 1640 media (AY27) or DMEM media (HT1376) supplemented with 10% fetal bovine serum, 1% penicillin (5000 units per mL) and streptomycin (5000 μL mL^{-1}) (Gibco, Invitrogen, Burlington, Canada), and maintained at 37 °C in 5% CO_2. Media used for culturing and plating cells contained phenol red; media used during PDT light irradiation contained neither phenol red nor sodium pyruvate. Cells were passaged at 80% confluence with media exchange every 2–3 days and used from passage number 6 to 27.

Imaging of cellular uptake

To determine cellular uptake of TLD1433 or b-Rutherrin, cells were plated in Nunc Labtek II 8-chamber slides (Cat#154534, Thermo Scientific, Waltham, MA, USA) at 40 000 cell per cm^2. NucBlue® Live was used as nuclear dye. Imaging was performed on a Zeiss confocal microscope (Zeiss LSM700, Jena, Germany). Multiple fields of view were imaged with separate channels for the nuclear dye ($\lambda_{ex} = 405$ nm, DAPI emission range), TLD1433 luminescence ($\lambda_{ex} = 488$ nm, longpass $\lambda_{em} = 630$ nm) and also a bright field. Quantitative analysis of luminescence was performed using Fiji software. Intensity histograms were obtained on a constant image stack, normalized for the cell number per image.

In vitro PDT

The cells in 200 μL media were plated at 10 000 cells per well in 96-well plates (Falcon, Invitrogen, CA, USA) 24 hours prior to PDT. Two plates were prepared for each experiment, with one for light exposure to establish cytotoxicity and one control plate without light for dark toxicity. For PDT, the media was replaced with phenol red- and pyruvate-free media plus TLD1433 or Rutherrin at varying concentrations of TLD1433 8–64 μM with the Tf fraction held at 5–10 μM. Rutherrin was incubated for 1 hour at 37 °C prior to adding to cell cultures, to allow for complex formation. Following 30 or 90 min PS incubation, excess TLD1433 or Rutherrin was removed and replaced with fresh phenol red and pyruvate-free media, followed by PDT light irradiation. The short incubation times were selected based on prior knowledge that a steady state is reached, and also the limited time available for bladder instillation during initial human trials.

Light activation of the PS was conducted using a 96-laser diode array light source (TLD 3000, Theralase Inc. Toronto, ON, Canada) by 625 nm light (119 mW cm^{-2}) for $H = 90 \pm 6$ J cm^{-2}. After irradiation, cells were returned to the dark in standard incubators for 20 hours.

Cell viability was measured by the Presto Blue Cell viability assay[41] quantifying fluorescence ($\lambda_{ex} = 560$ nm, $\lambda_{em} = 600$ nm) by using a plate reader. Dark toxicity reflects PS cell kill in the absence of light. Normalized PDT-mediated cell kill is total cell kill minus dark toxicity and light only toxicity.

MTD50

The toxicity and PDT response following TLD1433 and m-Rutherrin were evaluated *in vivo* as reported previously.[18] 8–10 week old BALB/C mice were used for *in vivo* experiments, carried out in accordance with the University Health Network guidelines (IACUC approval date 08/03/2012, assurance number A5408-01). Animals were housed with water and food supplied *ad libitum* at 12-hour day/night cycle.

The MTD50 for TLD1433 and m-Rutherrin was determined in non-tumor-bearing animals as described previously[18] fol-

lowing the Guidelines for the Testing of Chemicals.[42] Animal distress definition followed the classification of clinical signs given by the Federation for Laboratory Animal Science Associations guidelines.[19,40]

"*In vivo*" PDT

The subcutaneous CT26.CL25 tumor model was described previously.[18] When a tumor reached 5–6 mm, 12.5 μM of TLD1433 or m-Rutherrin in 100 μL 20% PG-saline were delivered *via* an intra-tumor (IT) injection using a syringe pump (#NE1000, New Era Pump Systems Inc., Farmingdale, NY, USA) at 0.01 mL min^{-1}. Intratumoral injection is among the established routes of photosensitizer delivery[75] and allows easy light delivery in the experimental model. After 4 hours, tumors were irradiated with light at 808 nm. The tumor was positioned above a 1.3 cm diameter aperture on a platform enabling light irradiation. A water blanket, set to ~30 °C, was lightly placed on top of the mouse to assist in removing heat due to optical energy absorbed by blood. Optical energy was delivered with an irradiance of 400 mW cm^{-2} for H = 600 J cm^{-2}. Mice were monitored daily and euthanized when tumors reached 10 × 10 mm, with Kaplan–Meier plots indicating days post PDT. PDT groups comprised 9 animals, except for the drug-only group (n = 2) and the light-only group (n = 3).

Statistical analysis

The effects of the Tf concentration and incubation time on dark toxicity and PDT effect were analyzed using two-way ANOVA, and differences between the specific groups were analyzed by *post-hoc* Tukey's multiple comparison test. The data are shown on a graph as mean (± standard error of the mean). LD_{50} with 95% confidence intervals were also calculated for PDT effect dose response curves by using a non-linear, sigmoid fitting model with a variable slope using GraphPad Prism 6.05. For *in vivo* survival analyses, Kaplan–Meier curves were established based on 9 mice for TLD1433 and Rutherrin, with significance (P = 0.05) tested by the Mantel–Cox test.

Results

Spectroscopic observations

Mixing of TLD1433 with water alone, incomplete, or complete cell culture media (Fig. 2A) demonstrated an increased molar extinction coefficient (M.E.C.) in complete media compared to

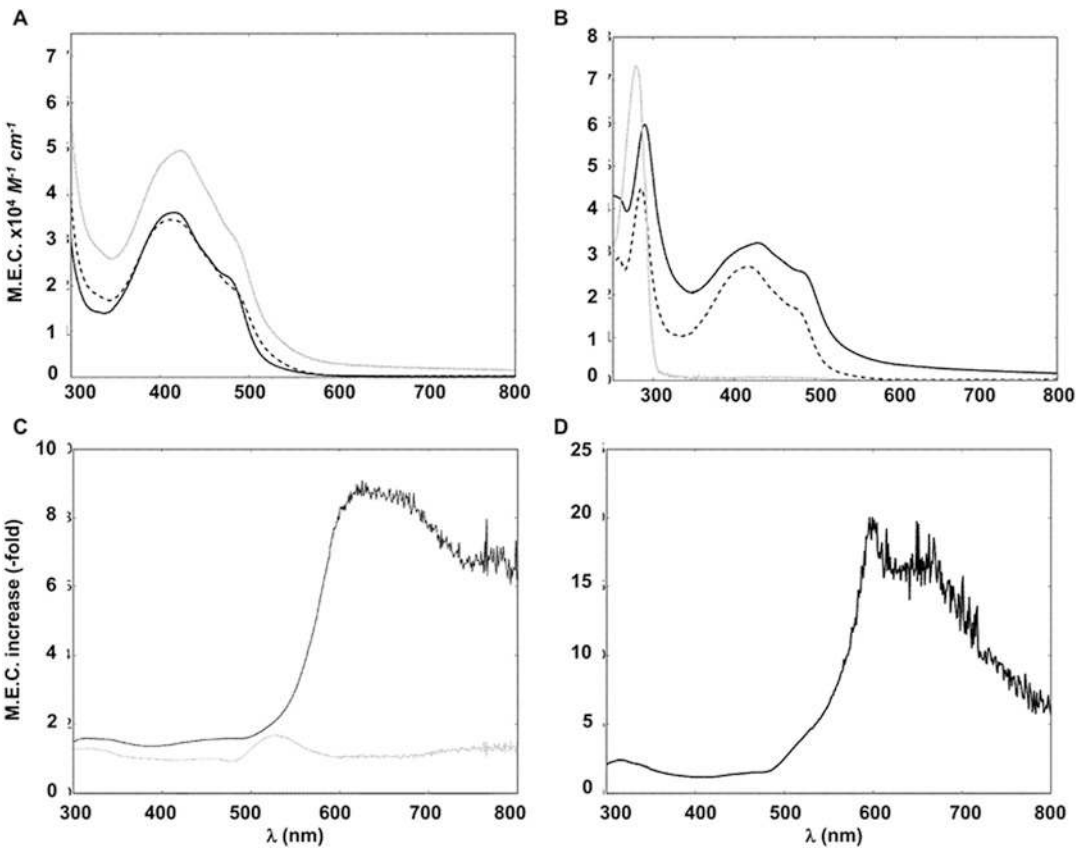

Fig. 2 Absorption changes of TLD1433 due to media composition and premixing with transferrin. (A, B) M.E.C. of TLD1433 in different media and following premixing with Tf. (A) 10 μM TLD1433 in DI-water (black), in incomplete DMEM (dashed black) and in complete DMEM (grey). (B) b-Tf (grey), 8 μM TLD1433 (dashed black), 8 μM b-Rutherrin (2.5 μM b-Tf) (light gray) in 10 mM phosphate buffer + 100 mM NaCl, pH = 7.2. (C, D) Ratios of M.E.C. (C) 10 μM TLD1433 in incomplete DMEM over water (grey) or in complete DMEM over incomplete DMEM (solid black). (D) 10 μM Rutherrin over 10 μM TLD1433. Data averages of n = 3–5 measurements.

the other solvents for the 500–800 nm range. The gain in molar extinction coefficient for complete *versus* incomplete media was 2.2, 9.1, and 6.4-fold at 530, 625, and 808 nm, respectively, whereas absorption of TLD1433 in incomplete media was not different from that of water (Fig. 2C), suggesting that protein components in complete media contributed to the observed absorption increase.

Fig. 2B shows the M.E.C. spectra for 10 μM b-Rutherrin (2.5 μM b-Tf), 2.5 μM b-Tf and 10 μM TLD1433 in phosphate buffer. The M.E.C. of Rutherrin increased at 280 nm and in the 450 to 520 nm range, reaching 4.3 times at 525 nm over TLD1433. Absorption in the 660 nm to NIR range, negligible for TLD1433 alone, was increased 16.5 times at 660 nm and 5.7 times at 808 nm (Fig. 2D).

The Rutherrin spectral Tf-binding signatures were similar for b-Tf and Tf (Fig. 3), and the Rutherrin signature was similar to that of TLD1433 in complete media. The signature of Rutherrin was similar to Fe^{3+} holo-Tf with the 400–500 nm maximum blue shifted (Fig. 3). TLD1433 was able to bind to holo-Tf although to a lesser extent at pH = 7.4 than in Rutherrin (Fig. 4).

M.E.C. of TLD1433 at 420 nm (corresponding to the peak spectral signature of TLD1433–Tf binding for Rutherrin) diminished with lower pH. The spectra of Rutherrin and TLD1433+holo-Tf demonstrated M.E.C. reduction however absorbance remained higher than for TLD1433 alone. Moreover, Rutherrin and TLD1433+holo-Tf increased in extinction at 420 nm at pH < 7 whereas holo-Tf–Fe^{3+} extinction reduced with lower pH, as anticipated (Fig. 4).

Spectral analysis showed immediate and stable TLD1433 association with holo-Tf, and while a similar rapid association with BSA was achieved, it spectrally reverted partially over 20 min post mixing of equal molar concentrations of the photosensitizer and protein. Monitoring the M.E.C. of the proteins, Tf and BSA, showed no pH dependence in their absorption at 270, 420, 600 and 800 nm. TLD1433 association with BSA and Tf resulted in no spectral changes at 270 and 420 nm due to acidification. The pH dependent M.E.C. losses at 530, 600 and 800 nm seen for the PS-Tf and TLD1433–BSA mirror those seen for TLD1433, hence spectroscopically there is no evidence for a dissociation of the TLD1433 and Tf for a pH as low as 3.17 whereas the M.E.C. of TLD1433 at all monitored wavelengths abruptly drops around 5.5 during acidification (data not shown). This suggests that the TLD1433–Tf complex association is strong enough to be maintained in the endosomes where Fe^{2+} and Tf dissociate.

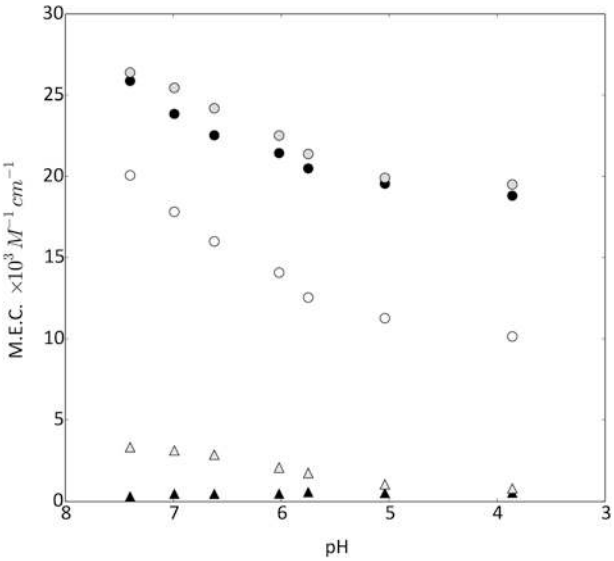

Fig. 4 Dependence of absorption of TLD1433, Rutherrin and transferrin on pH at 630 nm. 10 μM TLD1433 alone (white circles), 10 μM Rutherrin (10 μM apo-b-Tf, black circles) and 10 μM TLD1433 + 10 μM holo-b-Tf (grey circles) decreased their M.E.C. at lower pH. However, lowering the pH from 7.4 to 3.68 did not decrease the binding of 10 μM TLD1433 to 10 μM apo-b-Tf and to 10 μM holo-b-Tf suggesting that TLD1433 is not separated from Tf in this range of pH. The M.E.C. of 10 μM apo-b-Tf (black triangles) and 10 μM holo-b-Tf (grey triangles) is also shown. Magnitude of the binding signature can be derived upon subtracting M.E.C. of TLD1433 and also M.E.C. of apo-Tf and holo-Tf from the M.E.C. of Rutherrin and TLD1433+holo-b-Tf respectively. The plot suggests an increase in the signature magnitude at lower pH.

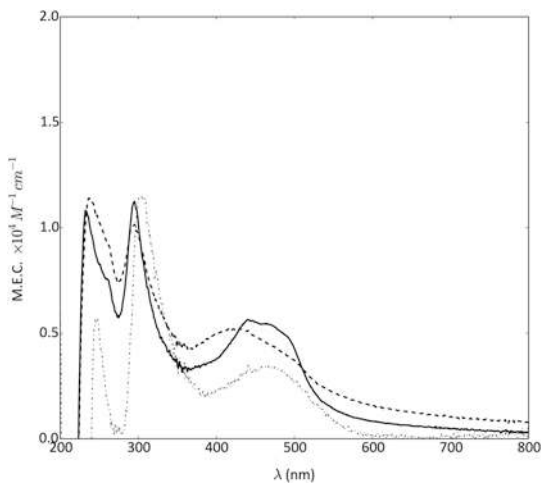

Fig. 3 TLD1433 binding signatures dependent on transferrin species. The Rutherrin (10 μM TLD1433) spectral Tf-binding signatures were similar for 10 μM b-Tf (dashed line) and 10 μM h-Tf (solid line) and similar but not identical to the signature of Fe^{3+} in 10 μM holo-Tf (gray dotted line). They were also similar to that of TLD1433 in complete media (see Fig. 2). Optically determined association between TLD1433 and b-Tf or holo-Tf was investigated in the pH range of 3.86 to 7.40 adjusted by adding 0.1 M HCl and verified by using a pH meter (Orion 3 Start, Thermo Scientific, MA, USA).

The increased Rutherrin absorption was reflected by increased luminescence emission compared to TLD1433 (Fig. 5). The emission maximum blue shifted 5 nm from 624 nm. While the molar extinction at 470 nm increased by a factor of ~1.5, luminescence emission increased three-fold, hinting at redistribution of the quantum yields determining a PS's de-excitation from its singlet excited state.

Photobleaching

The 525 nm irradiation-induced photobleaching of Rutherrin was lowered by approximately 15% after H = 200 J cm^{-2}

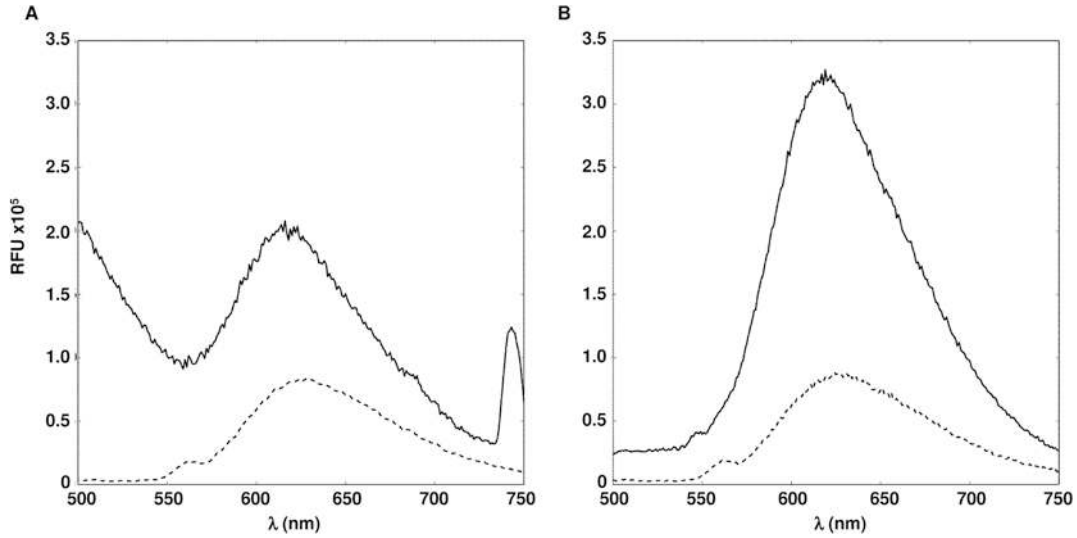

Fig. 5 Luminescence of TLD1433 and Rutherrin. Luminescence emission of 10 μM TLD1433 (dashed line) and 10 μM b-Rutherrin (2.5 μM b-Tf) (solid line) in PBS solution for (A) 380 nm and (B) 470 nm excitation. The peak at about 745 nm shown in Panel A indicates the 2nd diffraction of the excitation light.

(130 mW cm^{-2}) compared to TLD1433. Fig. 6 shows absorption changes at the activation wavelength as the function of photons absorbed with photobleaching reduced by approximately 50%. No spectral changes in the absorption spectra were observed across the entire spectral range.

ROS production in cell-free environment

ROS signals were corrected for the number of photons absorbed to generate comparable dose responses. Negligible or no ROS generation by TLD1433 alone was observed for 625 nm irradiation in water (Fig. 7). In the incomplete medium, virtually no $^1O_2$ generation (Fig. 8A), but considerable $^{\bullet}HO$ generation (Fig. 8B) was detected; in complete medium the $^1O_2$ signal was stronger and the $^{\bullet}HO$ signal was similar to the incomplete medium.

Rutherrin with 2.5 μM b-Tf induced improvements in the $^1O_2$ signal compared to the incomplete medium but no improvement in the $^{\bullet}HO$ signal. Rutherrin with 10 μM b-Tf induced a stronger $^1O_2$ signal and also a strong $^{\bullet}HO$ signal

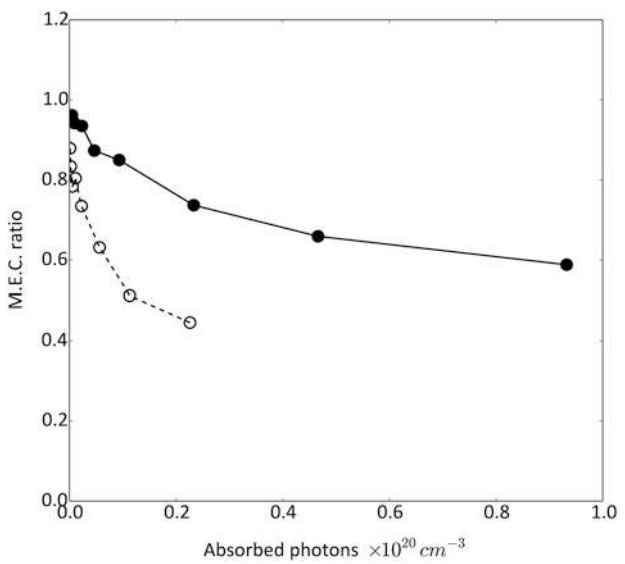

Fig. 6 Photobleaching of TLD1433 and Rutherrin. Photobleaching (% initial M.E.C.) of 10 μM TLD1433 (white circles) and 10 μM b-Rutherrin (2.5 μM Tf, black circles) both in 10 mM phosphate buffer + 100 mM NaCl, pH = 7.2 irradiated with 130 mW cm^{-2} at 530 nm.

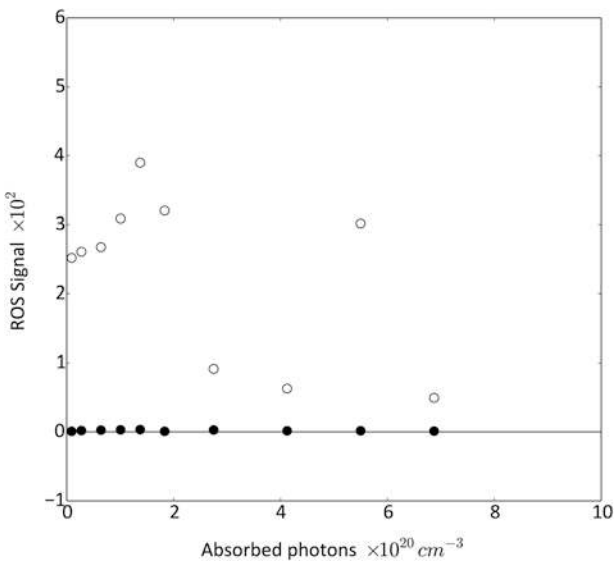

Fig. 7 Generation of ROS signal by TLD1433 in water under red light. ROS signal generated by TLD1433 alone for 625 nm (570 mW cm^{-2} irradiance) irradiation in water (open circles for singlet oxygen, black circles for hydroxyl radical indicator). Negligible to no ROS generation was observed.

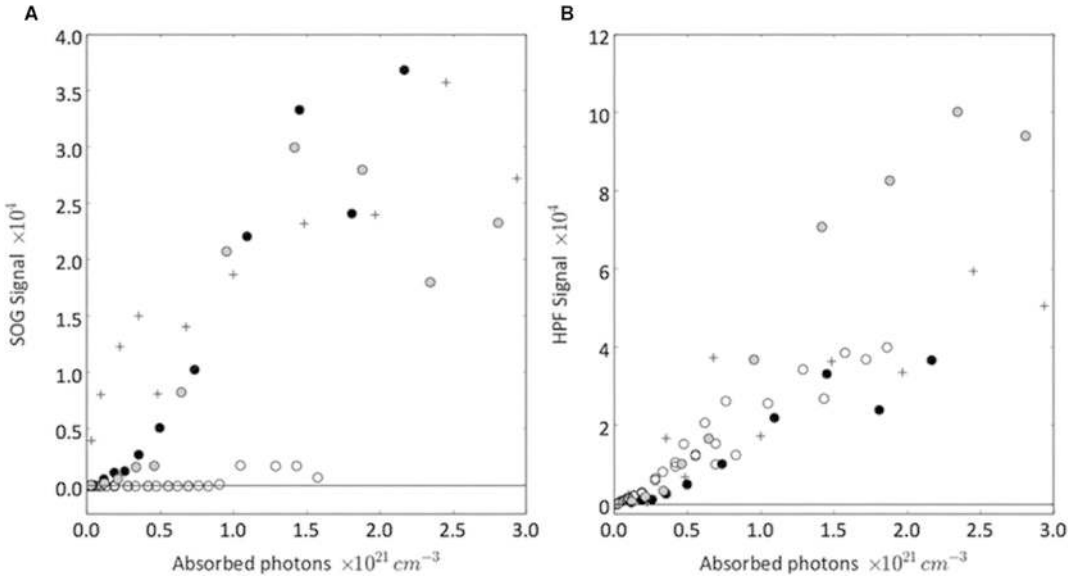

Fig. 8 Generation of ROS by TLD1433 and Rutherrin in DMEM under red light. Light mediated generation of ROS (625 nm, 570 mW cm^{-2} irradiance) using complete DMEM (crosses), 500 μM TLD1433 in incomplete DMEM (open circles) or 500 μM b-Rutherrin in incomplete DMEM with 2.5 μM b-Tf (black circles) or 10 μM b-Tf (gray circles), (A) $^1O_2$ and (B) $^{\bullet}HO$ indicators signal intensity.

compared to the incomplete medium. The ROS signals increased with the increase in the b-Tf concentration in Rutherrin. Also, while the presence of 2.5 μM b-Tf was enough to reproduce the $^{\bullet}HO$ signal in the complete medium, 10 μM b-Tf was required to reproduce a noticeable $^1O_2$ signal. During NIR (808 nm) irradiation (720 mW cm^{-2}, H < 600 J cm^{-2}), TLD1433 and Rutherrin in incomplete media generated no detectable $^1O_2$ signals and only a weak $^{\bullet}HO$ signal (Fig. 9).

Intracellular uptake

AY27 cells incubated in incomplete media or with Tf alone did not exhibit luminescence at 630 nm excitation after 40 minutes but after 150 minutes Rutherrin-incubated cells exhibited luminescence (630 nm) (Fig. 10) extending across the cytoplasm. After 150 min luminescence is mostly in proximity to the nuclear membrane. Frequency histograms of

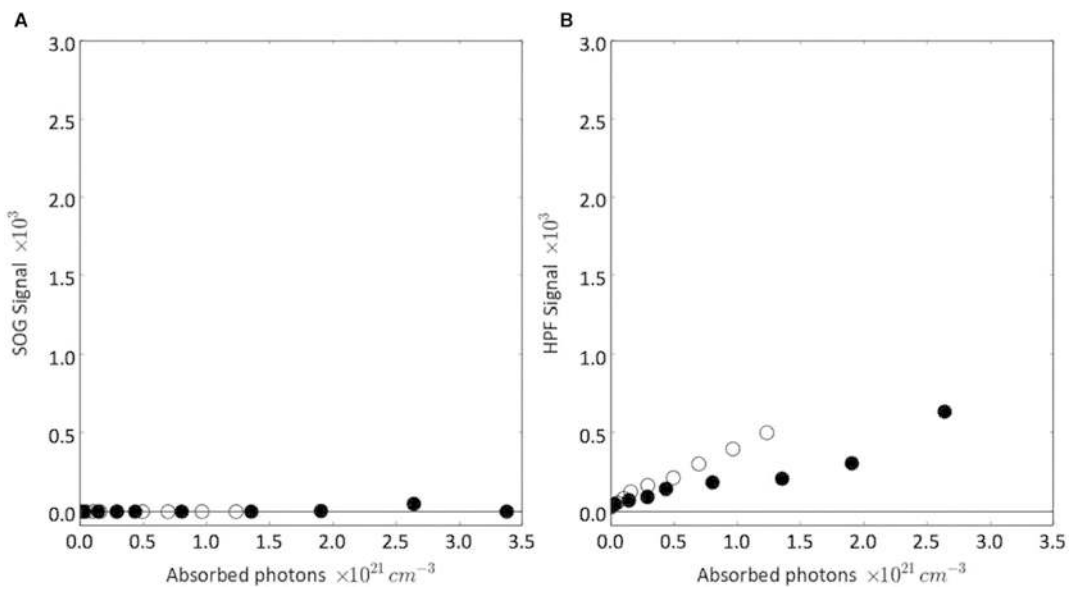

Fig. 9 Generation of ROS by TLD1433 and Rutherrin in DMEM under NIR light. Generation of ROS by 500 μM TLD1433 (open circles) or 500 μM b-Rutherrin (10 μM b-Tf, black circles) in incomplete DMEM upon irradiation with NIR light (808 nm, 720 mW cm^{-2}): (A) singlet oxygen and (B) HPF fluorescence as hydroxyl radical indicators.

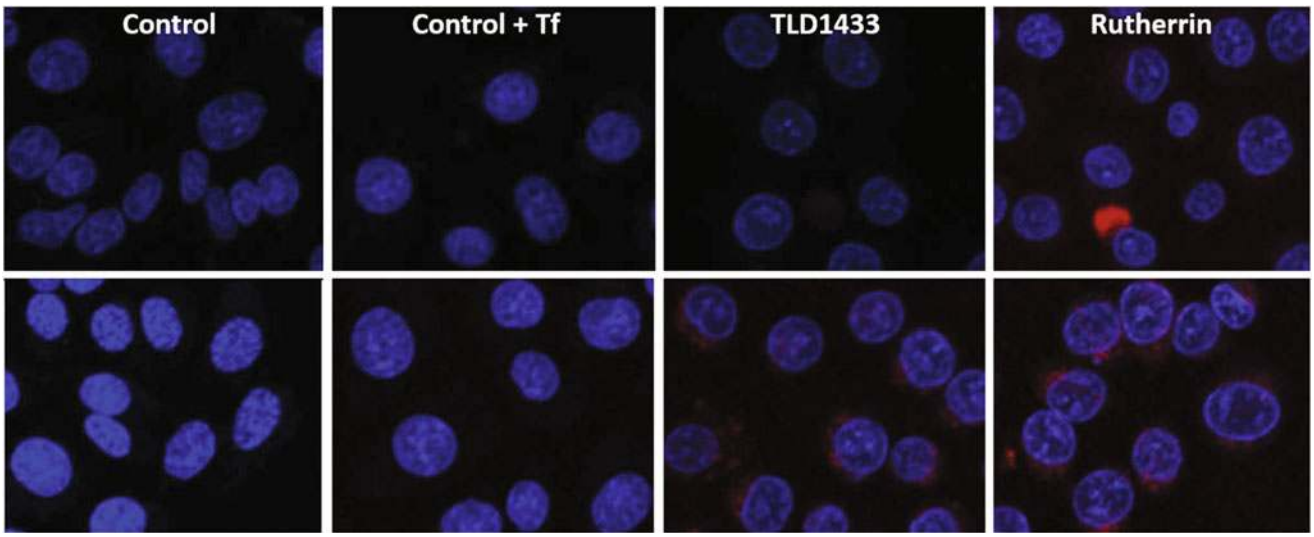

Fig. 10 Intracellular uptake of TLD433 and Rutherrin by AY27 cells. Uptake of 23.2 μM TLD1433 or 23.2 μM Rutherrin (10 μM Tf) by AY27 cells. Red luminescence (488 nm excitation) indicates the presence of the PS, blue fluorescence identifies nuclei. The images are shown for (top) 40 min and (bottom) 150 min incubation.

luminescence >630 nm showed an increased occurrence of high luminescence intensities [bits] following incubation with Rutherrin over TLD1433 (Fig. 11). Uptake of PS into the nuclei was not observed (Fig. 10). Bright field images showed alterations of the cell shape due to membrane blebbing at 40 and 150 min post TLD1433 incubation, whereas no blebbing is seen for Rutherrin (Fig. 12).

In vitro PDT

The PDT efficacy of TLD1433 and Rutherrin was concentration-dependent, whereby higher PS concentrations were associated with greater PDT-induced cell kill for 625 nm irradiation (Fig. 13). In AY27 cells, Rutherrin had an increased PDT effect compared to TLD1433, in particular observed for Rutherrin at 16–32 μM *versus* TLD1433 ($P < 0.001$), with improvement for 16 μM after 30 minutes and 32 μM after 90 minutes of incubation ($P < 0.05$). The concentration of Tf in Rutherrin did not affect the PDT effect. There was an additive effect of increased incubation time on the PDT effect of Rutherrin at 4–16 μM *versus* TLD1433 ($P < 0.05$–0.0001). Between-groups significant effects were observed only at 8 μM of TLD1433 in Rutherrin ($P < 0.05$–0.01). Improvement of PDT efficacy by Rutherrin was confirmed by a significantly lower LD_{50} at 30 min incubation, with a trend of reduced LD_{50} at 90 min incubation (Table 1).

Importantly, Rutherrin decreased dark toxicity in AY27 cells compared to TLD1433 over the 16–64 μM concentration range ($P < 0.01$–0.0001). Dark toxicity decreased for 16 μM Rutherrin after 30 and 90 minutes loading ($P < 0.01$–0.0001) and for 32–64 μM after 90 minutes loading ($P < 0.01$). Conversely, no significant impact of Rutherrin on either dark toxicity or PDT efficacy *versus* TLD1433 was observed in HT1376 cells (Fig. 14).

In vivo PDT

Determination of the MTD. Injection of Rutherrin containing 12.5 μM m-Tf increased the MTD dose to above 200 mg kg^{-1}, as compared to 110 mg kg^{-1} for TLD1433 alone[18] for IP administration, with all animals alive for 2 weeks.

PDT survival. Kaplan–Meier plots of tumor-bearing mice treated with TLD1433 or Rutherrin (12.5 μM m-Tf) mediated PDT at 808 nm (Fig. 15) show no significant survival increase for TLD1433 *versus* light only ($P = 0.179$) or PS dark toxicity ($P = 0.164$). Conversely, Rutherrin-mediated PDT showed an improvement survival compared to light only ($P = 0.0032$) and PS only ($P = 0.0182$), with a trend toward improved long-term survival for Rutherrin *versus* TLD1433-mediated PDT ($P = 0.0633$) with ~70% of animals surviving >90 days post-PDT. These data highlight 2 beneficial aspects of Rutherrin over TLD1433 mediated PDT: decreased systemic toxicity and improved post-PDT survival.

Discussion

There is intense research related to Ru^{2+} complexes as photosensitizers for PDT, as has been recently reviewed by Mari *et al.*[43] Some Ru-complexes have been shown to be excitable by NIR radiation so generally only in the context of multiphoton excitation.[44] Here an approach to achieve adequate NIR activation for cw light sources is presented, while simultaneously reducing dark toxicity.

Binding of TLD1433 to transferrin, forming Rutherrin, resulted in photophysical, pharmacokinetic, and toxicology improvements, making Rutherrin a more potent photosensitizing drug than TLD1433 alone. These effects include an

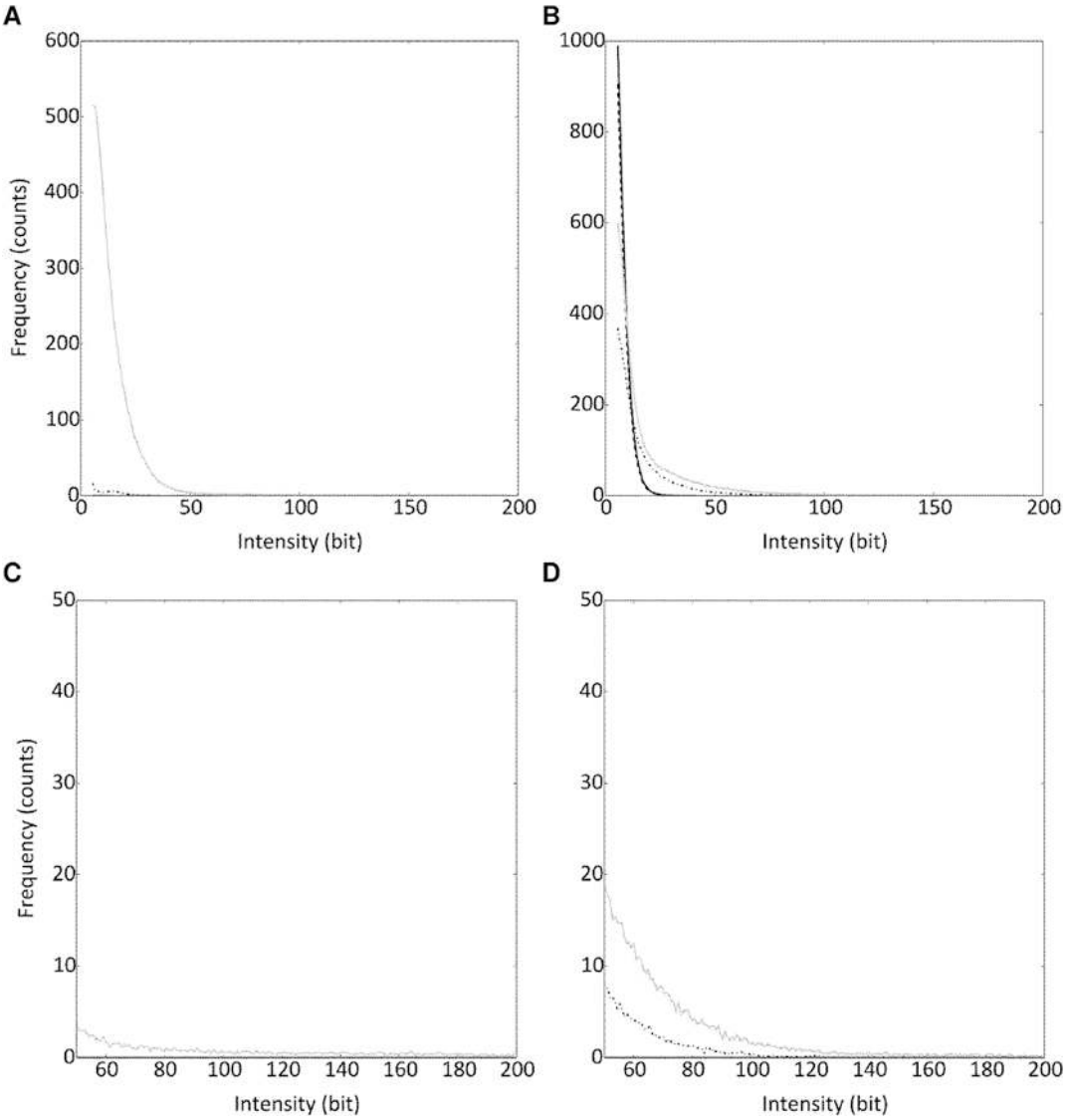

Fig. 11 Luminescence frequency profiles for Fig. 10 images. Luminescence (>630 nm) frequency histograms of images in Fig. 10, (A, C) after 40 min incubation and (B, D) after 150 min incubation. Controls (solid black), 10 μM Tf only (dashed black), 23.2 μM TLD1433 (dotted black) and 23.2 μM Rutherrin (10 μM Tf) (grey). Full histograms (A, B) and zoomed portion of them (C, D) are shown.

increased M.E.C. extending into the NIR, reduced dark toxicity *in vitro*, increased $^1O_2$ and $^{\bullet}HO$ generation quantum yield compared to TLD1433 alone in incomplete media, improved MTD *in vivo*, a cell line dependent improved PDT mediated cell kill and a trend towards increased therapeutic index *in vitro* and *in vivo*.

Binding of metal ions and metal-based compounds to Tf is well established, with Fe^{3+} binding to two specific binding pockets *via* electrostatic interactions[45] for pH > 5.5,[46] forming holo-Tf, and a detectable absorption increase at 280 nm, reflecting conformational changes by deprotonation of Tf,[47] and a new 430 nm absorption due to energy transfer between Fe^{3+} and Tf.[48] This was also noted upon adding TLD1433 to complete media or Tf generating Rutherrin. Additional absorption changes, attributable to TLD1433, were noted above 480 nm (Fig. 2). b-Rutherrin M.E.C. increased 4.5, 17.2 and 4.6-fold over TLD1433 at 530 nm, 625 nm and 808 nm, respectively.

The improved absorption beyond 625 nm opens the possibility for red and NIR-mediated PDT. Absorption increases depend on the actual complex that binds to transferrin. Arsene *et al.*[49] showed absorbance and luminescence loss upon binding of a Ru^{3+}-complex to proteins. The pH dependent spectroscopic studies indicated that Rutherrin remained intact even at pH < 5, suggesting the complex's intracellular integrity.

Stability of the TLD1433–protein adduct at low pH does not yet guarantee pH resistance of the improved absorbance in the PDT relevant range of wavelengths (green to NIR) that was attained *vs.* TLD1433 alone. The adduct may survive an acidified environment without retaining the same absorption properties.

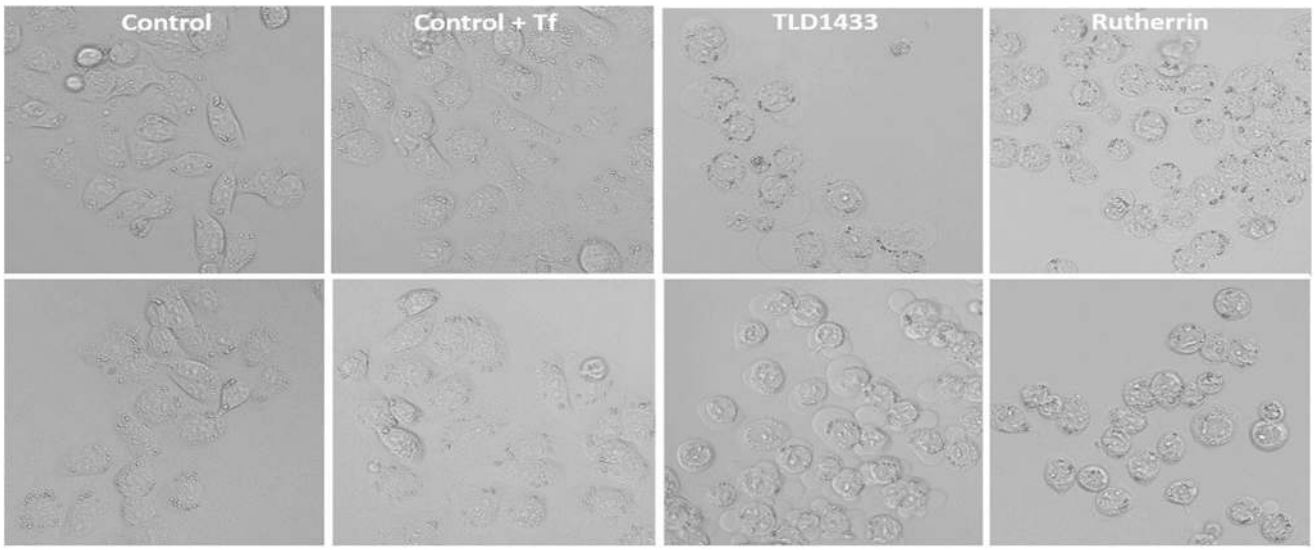

Fig. 12 Bright field images corresponding to Fig. 10 luminescent images. Bright field images of AY27 cells upon incubation with 23.2 μM TLD1433 or 23.2 μM Rutherrin (10 μM Tf). The images are collected after 40 min incubation time (top row) and after 150 min incubation time (bottom row). Cellular blebbing is visible for TLD1433 (third column from the left).

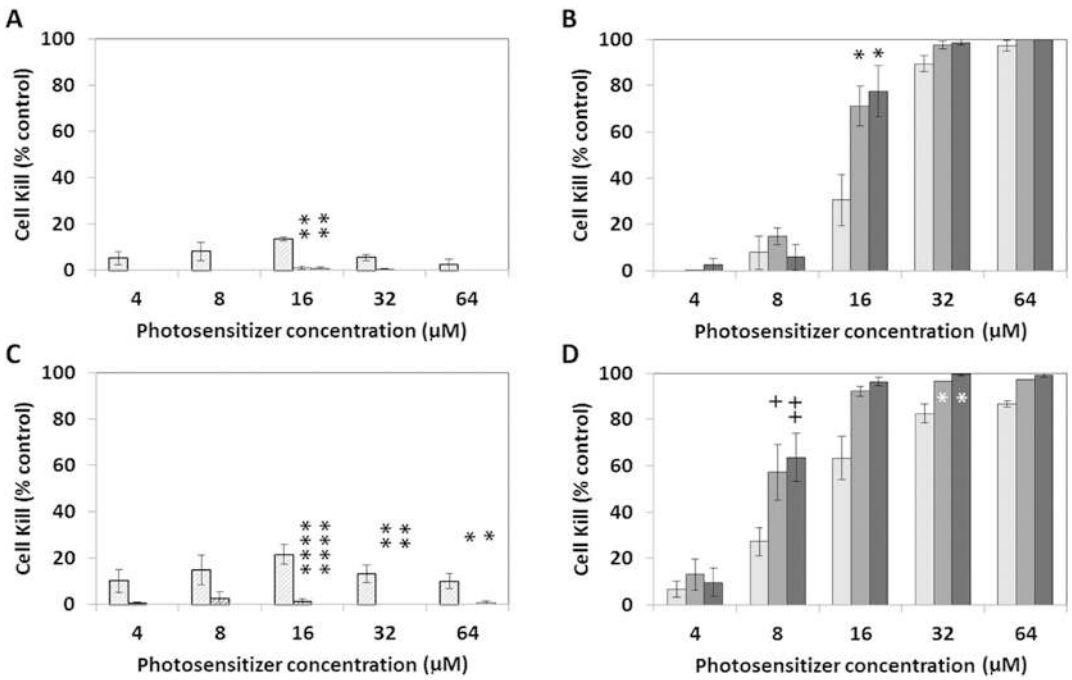

Fig. 13 Dark toxicity and PDT effect of TLD1433 and Rutherrin on AY27 cells. Concentration-dependent TLD1433 and 4–64 μM Rutherrin dark toxicity and PDT-mediated cell kill in rat AY27 cells as percent of control, following (A, B) 30 minutes or (C, D) 90 min incubation. (A, C) Dark toxicity, (B, D) following 625 nm light (119 mW cm^{-2}, 90 J cm^{-2}) mediated PDT for TLD1433 (light grey) and Rutherrin (5 μM Tf) (grey) or Rutherrin (10 μM Tf) (black). Asterisks indicate significant effect of Tf (*P < 0.05, **P < 0.01, ****P < 0.0001); crosses show significant effect of incubation time (+P < 0.05, ++P < 0.01, N = 3 for all groups).

The spectral signature of Rutherrin is stable at low pH suggesting stability of this TLD1433–apo-Tf adduct. Absorbance of Rutherrin is still increased *vs.* TLD1433 at low pH in the red and NIR range and retains a substantial part of absorbance improvement in the green range. A similar situation is observed with the TLD1433–holo-Tf adduct. Moreover, the magnitude of the signature peaks increases at low pH, probably in parallel with the loss of Fe^{3+} by holo-Tf. The TLD1433–BSA adduct demonstrates a pH-dependent decrease in the UV signature peak (associated with the protein conformation) but

Table 1 LD_{50} for dark toxicity and PDT effect on AY27 cells

	LD_{50} (μM)	95% CI	Dark/PDT ratio
Dark	>64.0		
PDT, 30 min incubation time			
TLD1433	17.0	13.5 to 21.4	>3.8
Rutherrin (5 μM Tf)	11.9	11.0 to 12.9*	>5.4
Rutherrin (10 μM Tf)	11.6	10.0 to 13.4*	>5.5
PDT, 90 min incubation time			
TLD1433	9.9	6.8 to 14.3	>6.5
Rutherrin (5 μM Tf)	6.5	4.9 to 8.6	>9.9
Rutherrin (10 μM Tf)	6.3	5.2 to 7.7	>10.1

NOTE: Dark LD_{50} is >64.0 μM for all experimental groups. Asterisks denote significant difference ($P < 0.05$) between TLD1433 and Rutherrin mediated PDT.

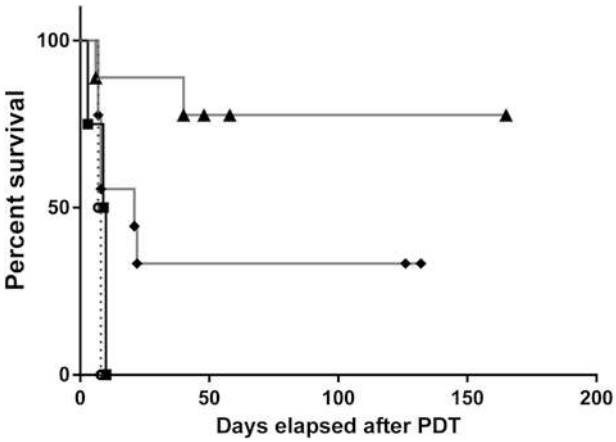

Fig. 15 *In vivo* effect of TLD1433 and Rutherrin mediated PDT. Tumor free survival after 50 mg per kg TLD1433 or m-Rutherrin (12.5 μM m-Tf) mediated PDT in the CT26.CL25 subcutaneous tumor model. For NIR PDT 5 × 5 mm tumors were treated with H = 600 J cm^{-2} 808 nm photons. Light only (squares), TLD1433 only (circles), TLD1433 PDT (rhombuses), Rutherrin PDT (triangles).

stability of the blue range peak (associated with interaction between Ru^{2+} and protein). The TLD1433+BSA adduct retains absorbance gain at low pH in the red and NIR range and partly retains it in the green range. This suggests that the absorbance gain in the visible-NIR range attained by Rutherrin and TLD1433–BSA adducts can completely resist low pH occurring in endosomes while demonstrating pH-resistant signatures of TLD1433–protein binding.

Thus, while the intracellular transport of the PS remains somewhat uncertain and its accumulation outside the nucleus due to the properties of the relatively much larger Tf is likely. It is rather certain that Rutherrin will retain the favourable optical properties intracellularly also. Transition metal binding to Tf has been shown for other ions[50–54] and complexes[55,56] including Ru^{2+} [57] and Ru^{3+} [39,58–61] compounds. Ru^{2+} complexes bind electrostatically[62] or *via* a N-donor[57] whereas Ru^{3+} complexes produce covalent metal–protein

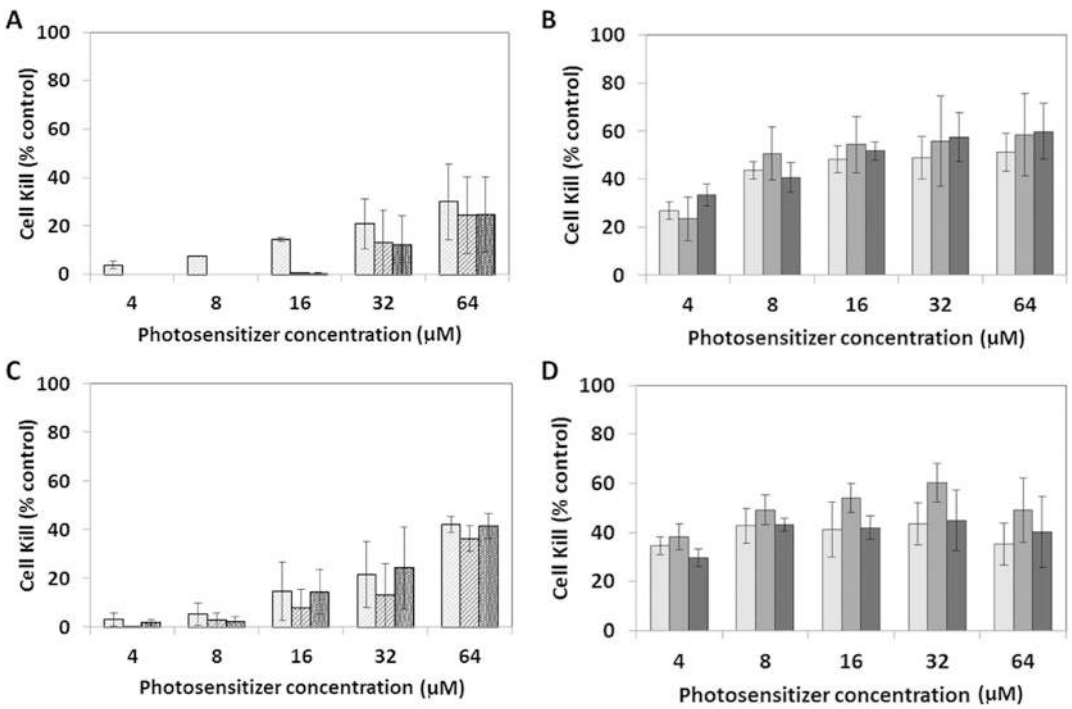

Fig. 14 Dark toxicity and PDT effect of TLD1433 and Rutherrin on HT1376 cells. Concentration-dependent TLD1433 and 4–64 μM Rutherrin dark toxicity and PDT-mediated induced cell kill in human HT1376 cells following (A, B) 30 min or (C, D) 90 min incubation. (A, C) Dark toxicity, (B, D) following 625 nm light (119 mW cm^{-2}, 90 J cm^{-2}) mediated PDT for TLD1433 (light grey) and Rutherrin (5 μM Tf) (grey) or Rutherrin (10 μM Tf) (black). N = 2 for all groups.

conjugates[58–60] retained intracellularly.[63] While bicarbonate is essential for Fe^{3+} Tf binding,[64] it is not required for TLD1433 binding as also shown for other Ru^{2+} complexes.[65] High binding ratios between metal complexes and Tf have been reported[49,63,66] and Ru^{2+} complexes can bind to Tf independently of Fe^{3+}.[57,62,67] For the molar ratios of TLD1433 and Tf employed here binding appears complete, while not introducing an excessive load of Tf into the biological system. Some Ru^{2+} complexes bind stronger to the holo-Tf than apo-Tf, increasing with the number of metal ions in the complex,[62] while Ru complexes may be cooperative in Tf binding with Fe^{3+} to Tf for higher cellular accumulation.[68] The reduced dark *in vivo* toxicity suggests that mixing of TLD1433 with Tf prior to administration improves the supply of Fe^{3+} to the cells as it does not deplete Tf.

TLD1433 binds to both apo-Tf and holo-Tf with binding signatures less pronounced for the holo-Tf at pH = 7.4, probably due to prior Fe^{3+} binding (Fig. 4). This is in contrast to the improved binding of Ru^{3+} based NAMI-A to the holo-Tf compared to apo-Tf.[31] Nevertheless, successful binding of TLD1433 to the holo-Tf can have positive clinical implications because recognition of the holo-Tf by Tf-R is guaranteed in comparison with apo-Tf, ensuring active uptake of the PS into cells.

There is no evidence that TLD1433 displaces Fe^{3+} from the holo-Tf upon binding, because the difference between signature peaks for TLD1433–apoTf and TLD1433–holoTf is less than the magnitude of the signature peak of Fe^{3+} in the holo-Tf. Also, subtracting of the signature of TLD1433–holoTf from the signature of Rutherrin does not provide a spectrum characteristic for free Fe^{3+} ions (data not shown). This is in accordance with the literature data indicating that binding of Ru^{2+} complexes does not affect Tf conformation, similarly to the binding of Zn^{2+} and Cu^{2+} ions.

While Rutherrin does not disrupt Tf-mediated Fe^{3+} dependent physiological activities and indeed the Ru^{2+} is not known to achieve the conformational change in Tf required for its recognition by Tf-R, hence, binding of both TLD1433 and Fe^{3+}, or the use of apo-Tf is required. Ru^{3+} complexes have been shown to bind holo-Tf at a 20 : 1 ratio,[31] whereas TLD1433 binds the holo-Tf only at a premix stoichiometry of 2 : 1. TLD1433 binding to both apo- and holo-Tf was not disrupted by low pH, unlike binding of Fe^{3+} to the holo-Tf, indicating that TLD1433 remains bound to Tf after intracellular uptake, thus retaining improved absorbance and ROS generating properties, leading to improved PDT efficacy. Retaining of TLD1433 binding to Tf at low pH suggests Fe^{3+} site-independent covalent binding. For example, it was shown that NAMI-A does not displace Fe^{3+} upon binding to holo-Tf and that binding is irreversible at pH = 7.0.[31] However, NAMI-A's activity is not photomediated and binding to proteins decreases its efficacy *in vivo* and *in vitro*,[69] whereas our study demonstrates the possibility of improved photoactive efficacy by TLD1433 upon protein binding.

Some studies suggest that Ru^{2+} complexes conjugated to Tf can be released from endosomes into cytosol and further to nucleus.[54] However, Tf remains normally bound to Tf-R at low pH upon endocytosis, which is essential for the recycling of Tf back to extracellular space while Fe^{3+} is released into cytosol and is further transported to mitochondria.[77] Hence, PDT-mediated activation of the photosensitizer is more likely to occur in endosomes containing Rutherrin bound to TfR. This possibility has been indicated by Dobrucki.[78]

The luminescence intensity gain by Rutherrin (3.3-fold) exceeds the extinction gain at 470 nm, suggesting a change in the relative contributions of luminescence, internal conversion and triplet state quantum yields. The quantum yields vary with the solvent, suggesting ionic concentration and pH as confounders to ROS production.

Rutherrin had a 40–50% reduced photobleaching rate over TLD1433 in PBS and better than for TLD1433 with BSA, both providing alternative ROS targets,[18] whereby Tf is likely more efficient due to direct physical proximity to the ROS source. Exposure of Tf to ROS does not affect TLD1433 binding to Tf as no spectral changes are observed post irradiation (data not shown).

Rutherrin-reduced photobleaching over TLD1433 is advantageous in PDT as it increases the PS's ability to generate more ROS for a fixed concentration.[70]

ROS generation by TLD1433 was measured in three different solvent environments. DMEM supplemented by FBS and antibiotics (complete DMEM) emulated an extracellular environment containing ions, low molecular weight organic molecules and proteins (including Tf). Incomplete medium (with supplementation by FBS and antibiotics) was used to preserve ionic and low molecular weight components but to exclude Tf (and other proteins). Finally, water was used as a simplest solvent devoid of both ionic and organic components. Tf was added to the incomplete DMEM to elucidate the specific role of Tf in ROS production. For TLD1433, $^{\bullet}HO$ generation dominates over $^1O_2$, which is indicative of a type I photoreaction. Proteins in complete DMEM improved $^1O_2$ but not $^{\bullet}HO$ generation. In contrast, b-Rutherrin containing 2.5 μM b-Tf, at concentrations equivalent to Tf in complete media, did not improve $^1O_2$ to the extent of complete media, requiring 10 μM b-Tf to achieve this. This suggests a role of other components (salts, proteins, and small organic molecules) in improved ROS generation in complete medium. Further the b-Tf concentration increase resulted in an increased $^{\bullet}HO$ generation also (Fig. 8).

Improved ROS generation by Rutherrin as a function of radiant exposure reflects its increased M.E.C. over TLD1433. For red and NIR activation wavelengths, ROS generation showed a nonlinear increase as a function of radiant exposure (see Fig. 8 and 9), suggesting the presence of other factors, such as an absorbed energy threshold, for detectable ROS generation as the real ROS yield may be underreported due to the bicarbonate acting as an electron acceptor reducing hydroxyl generation. ROS quantum yield modifiers are also suggested by the higher $^1O_2$ production in complete media *versus* Rutherrin containing similar concentrations of Tf.

In vitro experiments were executed using bladder cancer cell lines as bladder cancer is an obvious first target for clinical translation using intracavity instillation to minimize systemic toxicity, particularly due to the high Tf-R expression in these tumours.[14]

The predominant type I photoreaction observed following 625 nm and 808 nm irradiation can facilitate an added *in vivo* advantage due to the longer lifetime of $^{\bullet}HO$ in biological systems, findings which could also explain the Type I PDT observed previously[39] for a comparable Ru^{2+} compound. Mixed Type I/II photoreaction has been reported previously,[71,72] with $^{\bullet}HO$ being a reaction product of $^1O_2$.[73]

Intracellular luminescence of TLD1433 and Rutherrin in cell cultures (Fig. 10 and 11) indicates rapid uptake of Rutherrin co-localizing with organelles proximal to the nucleus, whereby for short incubation times the fluorescence intensity difference exceeds the anticipated higher fluorescence due to increased absorption coefficient and increased fluorescence quantum yield. For prolonged incubation of 150 min, no significant increase in cellular luminescence was observed beyond that anticipated due to the higher attenuation coefficient, nor evidence of nuclear localization of TLD1433 or Rutherrin, as reported for similar complexes in HL-60 cells.[17] Lack of nuclear localization speaks against DNA damage as a primary mechanism of action, despite report of TLD1433 cleaving DNA plasmids in solution.[17] While Ru^{2+}-based PSs have been shown to localize in the nucleus[43] significant fractions remained in the cytosol and organelles, primarily in mitochondria.[68,70,74] The absence of nuclear localization precludes DNA damage as a mechanism of action but also prevents undesirable oncogenic modifications. There was noticeable luminescence of Rutherrin (10 μM Tf) but not of TLD1433 40 minutes after loading. Taking into consideration the higher luminescence emission, this indicates an active uptake of Rutherrin. Rutherrin appeared to protect cells from short-term stress such as membrane blebbing induced by TLD1433 incubation (Fig. 12). At 150 min, the luminescence is similar between the two PSs, so considering the higher molar extinction for Rutherrin, 2 effects can be the root cause. Rutherrin remains intact and TLD1433 equally binds to proteins with improved absorption and hence the higher luminescence does translate into a higher drug concentration. Should TLD1433 remain unbound to Tf at pH < 5.5 luminescence may not indicate a higher PS concentration. Therefore, the improved PDT effects for AY27 cells are due to a higher efficacy or higher concentration. Luminescence for TLD1433 observed at 150 minutes can be due to passive diffusion following membrane blebbing (Fig. 12).

TLD1433 is a powerful photosensitizer, with red light PDT LD_{50} as low as 4 μM and PDT-mediated cell kill as high as 1.35 logs of cell kill for U87 human glioblastoma cells and 1.2 logs of cell kill for HT1376 cells (data not shown). In the present study, TLD1433 PDT efficacy in red light reached 1.55 logs cell kill and was limited by the photon density provided.

Moreover, in green light (532 nm) PDT mediated LD_{50} for TLD1433 was <1 nM for radiant exposure (H) > 90 J cm^{-2}.[18] The PDT LD_{50} of 4 μM for red activation or in the sub nM region for 525 nm excitation compared favourably against other Ru^{2+} polypyridyl complexes[27]

Rutherrin further increased PDT efficacy at constant H compared to TLD1433 for AY27 cells after 30 and 90-minute incubation. Conversely, there was virtually no PDT efficacy improvement for HT1376 cells, requiring further testing of cell lines and their Tf-R status. Incubation times <2 hours are preferable to maximize the therapeutic ratio between dark and PDT toxicity for both TLD1433 and Rutherrin and uptake is faster for Rutherrin.

Improved PDT efficacy of Rutherrin at constant H is novel for this complex and different from prior results.[69] It is noteworthy that 5 μM Tf is sufficient to ensure this improvement by intracellular transport of TLD1433 bound to Tf, as a further increase of the Tf concentration does not increase PDT efficacy. Increased Rutherrin efficacy *in vitro* (Fig. 13 and 14) translated into *in vivo* studies, as demonstrated by an increased survival rate after Rutherrin mediated NIR-PDT (Fig. 15). This is in accordance with the findings that while Rutherrin has higher activity in *in vitro* PDT and ROS production under red light, it retains some ROS production capacity under NIR light. Retention of the NIR activity also suggests that Rutherrin remains intact within the cell. The high *in vivo* NIR mediated PDT survival was not predicted based on experiments producing little ROS in a cell-free environment, suggesting that high *in vivo* NIR-PDT efficacy may be subjected to other mediators, beyond the increased M.E.C. at 808 nm as seen in Fig. 2.

While the M.E.C at 525 nm is about an order of magnitude higher than at 808 nm, see Fig. 2, the photon density delivered by the experiments reported by Fong *et al.*[18] using 525 nm was 4.8 times lower (5.07×10^{20} $h\nu$ *versus* 2.44×10^{21} $h\nu$ for 192 J cm^{-2} at 525 nm *versus* 600 J cm^{-2} at 808 nm, respectively) and if the two wavelengths resulted in the same ROS quantum yield, PDT with 525 nm should have generated about twice the ROS concentration than the 808 nm mediated PDT, albeit in a shallower volume. Hence, with the longer wave yielding a lower ROS concentration the improved tissue penetration proved beneficial. Additionally, the comparison between TLD1433 and Rutherrin efficacy becomes less tumour size dependent.

The CT26.CL25 cells used in the *in vivo* model tumor presented the beta galactosidase antigen and hence were able to induce an anti-tumor immunological response. This, however, does not prevent the tumor growth in the absence of PDT treatment. Moreover, tumor destruction and tumor growth suppression following Rutherrin-mediated PDT were improved compared to the PDT mediated by TLD1433. This suggests a direct facilitating effect of Rutherrin on tumor-free survival of the animals rather than the potential anti-tumor immunological effect.

It is noteworthy that premixing of TLD1433 with Tf results in improved intracellular uptake and PDT efficacy both *in vitro* and *in vivo* despite albumin being present in the culture medium *in vitro* and in extracellular fluids *in vivo* at a concentration higher than that of Tf and Tf must therefore be a stron-

ger binding competitor. It is known that some Ru^{2+} complexes bind to albumin, most likely by covalent bonds, with a likely stoichiometry of 6–7 : 1.[77] Moreover, binding of Ru^{2+} complexes to albumin was stronger than to apo-Tf and comparable to that of holo-Tf.[79] Our data confirm that binding of TLD1433 to albumin is not less than the binding to Tf by the magnitude of spectral signature peaks and results in a greater absorbance increase in the green to NIR range that is also resistant to acidification at pH = 5.5. However, the presence of albumin does not preclude the PDT effect of TLD1433, and additional Tf (producing Rutherrin) further improves the PDT effect both *in vitro* and *in vivo*. Moreover, a low pH-resistant increase in absorbance in the green to NIR range upon premixing TLD1433 with albumin can be beneficial for the PDT effect independently on the Tf-associated uptake of the PS into cells. Finally, in the case of Rutherrin injection as a part of PDT treatment, TLD1433 is unlikely to be bound by albumin.

Conclusions

Our findings suggest a beneficial role of Rutherrin as an active PDT PS drug over TLD14433 alone, as the premix with Tf increases the molar extinction from 400 to 850 nm, photobleaching resistance, ROS production, rapid intracellular uptake, and *in vivo* PDT efficacy, while decreasing *in vivo* toxicity. The predominant generation of hydroxyl radicals is an indication for its use in the low oxygen environment present in solid tumors. The combination of Tf-mediated transport and PDT activity at a low oxygen concentration due to the dual energy or charge transfer mechanism is an interesting aspect towards targeting cancer stem cells as previously proposed for glioma stem cells[75] and leukemia.[76,77]

Acknowledgements

Theralase Inc., the employer of Pavel Kaspler, Savo Lazic, Yaxal Arenas and Arkady Mandel is evaluating and developing the ruthenium based photosensitizer TLD1433 for clinical applications and financially supported this study. The work was conducted at the University Health Network, Toronto, Canada. The study obtained partial support through the Ontario Ministry of Health and Long Term Care.

References

1 R. Bonnett, *Chemical aspects of photodynamic therapy*, Gordon and Breach Science Publishers, Amsterdam, The Netherlands, 2000.
2 M. Ethirajan, Y. Chen, P. Joshi and R. K. Pandey, *Chem. Soc. Rev.*, 2011, **40**, 340–362.
3 D. E. J. G. J. Dolmans, D. Fukumura and R. K. Jain, *Nat. Rev. Cancer*, 2003, **3**, 380–387.
4 J. C. Kennedy, R. H. Pottier and D. C. Pross, *J. Photochem. Photobiol., B*, 1990, **6**, 143–148.
5 Z. Huang, Q. Chen, D. Luck, J. Beckers, B. C. Wilson, N. Trncic, S. M. Larue, D. Blanc and F. W. Hetzel, *Lasers Surg. Med.*, 2005, **36**, 390–397.
6 K. L. Molpus, D. Kato, M. R. Hamblin, L. Lilge, M. Bamberg and T. Hasan, *Cancer Res.*, 1996, **56**, 1075–1082.
7 J. T. Elliott, K. S. Samkoe, J. R. Gunn, E. E. Stewart, T. B. Gardner, K. M. Tichauer, T.-Y. Lee, P. J. Hoopes, S. P. Pereira, T. Hasan and B. W. Pogue, *Acad. Radiol.*, 2015, **22**, 572–579.
8 B. W. Engbrecht, C. Menon, A. V. Kachur, S. M. Hahn and D. L. Fraker, *Cancer Res.*, 1999, **59**, 4334–4342.
9 D. Przybyla, C. Göbel, A. Imboden, M. Hamberg, I. Feussner and K. Apel, *Plant J.*, 2008, **54**, 236–248.
10 S. Lee, D. H. Vu, M. F. Hinds, S. J. Davis, A. Liang and T. Hasan, *J. Biomed. Opt.*, 2008, **13**, 064035.
11 H. Kobuchi, K. Moriya, T. Ogino, H. Fujita, K. Inoue, T. Shuin, T. Yasuda, K. Utsumi and T. Utsumi, *PLoS ONE*, 2012, **7**, e50082.
12 K. Inoue, T. Karashima, M. Kamada, T. Shuin, A. Kurabayashi, M. Furihata, H. Fujita, K. Utsumi and J. Sasaki, *Pathobiology*, 2009, **76**, 303–314.
13 K. Berg, P. K. Selbo, A. Weyergang, A. Dietze, L. Prasmickaite, A. Bonsted, B. Ø. Engesaeter, E. Angell-Petersen, T. Warloe, N. Frandsen and A. Høgset, *J. Microsc.*, 2005, **218**, 133–147.
14 A. O. Abu-Yousif, A. C. E. Moor, X. Zheng, M. D. Savellano, W. Yu, P. K. Selbo and T. Hasan, *Cancer Lett.*, 2012, **321**, 120–127.
15 A. M. Master, M. Livingston, N. L. Oleinick and A. Sen Gupta, *Mol. Pharm.*, 2012, **9**, 2331–2338.
16 Y. Liu, R. Hammitt, D. A. Lutterman, L. E. Joyce, R. P. Thummel and C. Turro, *Inorg. Chem.*, 2009, **48**, 375–385.
17 G. Shi, S. Monro, R. Hennigar, J. Colpitts, J. Fong, K. Kasimova, H. Yin, R. DeCoste, C. Spencer, L. Chamberlain, A. Mandel, L. Lilge and S. A. McFarland, *Coord. Chem. Rev.*, 2015, **282**, 127–138.
18 J. Fong, K. Kasimova, Y. Arenas, P. Kaspler, S. Lazic, A. Mandel and L. Lilge, *Photochem. Photobiol. Sci.*, 2015, **11**, 2014–2023.
19 S. Monro, J. Scott, A. Chouai, R. Lincoln, R. Zong, R. P. Thummel and S. A. McFarland, *Inorg. Chem.*, 2010, **49**, 2889–2900.
20 E. Wachter, D. K. Heidary, B. S. Howerton, S. Parkin and E. C. Glazer, *Chem. Commun.*, 2012, **48**, 9649–9651.
21 E. C. Glazer, *Isr. J. Chem.*, 2013, **53**, 391–400.
22 A. A. Holder, D. F. Zigler, M. T. Tarrago-Trani, B. Storrie and K. J. Brewer, *Inorg. Chem.*, 2007, **46**, 4760–4762.
23 Y. Sun, L. E. Joyce, N. M. Dickson and C. Turro, *Chem. Commun.*, 2010, **46**, 6759.
24 Y. Sun, L. E. Joyce, N. M. Dickson and C. Turro, *Chem. Commun.*, 2010, **46**, 2426.
25 B. S. Howerton, D. K. Heidary and E. C. Glazer, *J. Am. Chem. Soc.*, 2012, **134**, 8324–8327.
26 Q.-X. Zhou, W.-H. Lei, Y. Sun, J.-R. Chen, C. Li, Y.-J. Hou, X.-S. Wang and B.-W. Zhang, *Inorg. Chem.*, 2010, **49**, 4729–4731.

27 C. Mari, V. Pierroz, R. Rubbiani, M. Patra, J. Hess, B. Spingler, L. Oehninger, J. Schur, I. Ott, L. Salassa, S. Ferrari and G. Gasser, *Chem. Eur. J*, 2014, **20**, 14421–14436.
28 D. S. McClure, *J. Chem. Phys.*, 1949, **17**, 665.
29 J. Pérez-Prieto, L. P. Pérez, M. González-Béjar, M. A. Miranda and S.-E. Stiriba, *Chem. Commun.*, 2005, 5569.
30 O. Dömötör, C. G. Hartinger, A. K. Bytzek, T. Kiss, B. K. Keppler and E. A. Enyedy, *J. Biol. Inorg. Chem.*, 2013, **18**, 9–17.
31 K. Śpiewak and M. Brindell, *JBIC, J. Biol. Inorg. Chem.*, 2015, **20**, 695–703.
32 A. Levina, A. Mitra and P. A. Lay, *Met. Integr. Biometal Sci.*, 2009, **1**, 458–470.
33 S. Tortorella and T. C. Karagiannis, *Curr. Drug Delivery*, 2014, **11**, 427–443.
34 S. Tortorella and T. C. Karagiannis, *J. Membr. Biol.*, 2014, **247**, 291–307.
35 A. S. L. Derycke, A. Kamuhabwa, A. Gijsens, T. Roskams, D. De Vos, A. Kasran, J. Huwyler, L. Missiaen and P. A. M. de Witte, *J. Natl. Cancer Inst.*, 2004, **96**, 1620–1630.
36 P. G. Cavanaugh, *Breast Cancer Res. Treat.*, 2002, **72**, 117–130.
37 W. M. Sharman, J. E. van Lier and C. M. Allen, *Adv. Drug Delivery Rev.*, 2004, **56**, 53–76.
38 E. Paszko, G. M. F. Vaz, C. Ehrhardt and M. O. Senge, *Eur. J. Pharm. Sci.*, 2013, **48**, 202–210.
39 Y. Arenas, S. Monro, G. Shi, A. Mandel, S. McFarland and L. Lilge, *Photodiag. Photodyn. Ther.*, 2013, **10**, 615–625.
40 W. E. Jones, R. A. Smith, M. T. Abramo, M. D. Williams and J. Van Houten, *Inorg. Chem.*, 1989, **28**, 2281–2285.
41 T. S. Istivan, E. Pirogova, E. Gan, N. M. Almansour, P. J. Coloe and I. Cosic, *PLoS ONE*, 2011, **6**, e24809.
42 OECD, 1981.
43 C. Mari, V. Pierroz, S. Ferrari and G. Gasser, *Chem. Sci.*, 2015, **6**, 2660–2686.
44 B. Yu, C. Ouyang, K. Qiu, J. Zhao, L. Ji and H. Chao, *Chem. Eur. J*, 2015, **21**, 3691–3700.
45 C. D. Quarles Jr., K. M. Randunu, J. L. Brumaghim and R. K. Marcus, *Metallomics*, 2011, **3**, 1027.
46 J. Williams and K. Moreton, *Biochem. J.*, 1980, **185**, 483–488.
47 R. J. Hilton, M. C. Seare, N. D. Andros, Z. Kenealey, C. M. Orozco, M. Webb and R. K. Watt, *J. Inorg. Biochem.*, 2012, **110**, 1–7.
48 N. G. James, J. A. Ross, A. B. Mason and D. M. Jameson, *Protein Sci.*, 2010, **19**, 99–110.
49 A. L. Arsene, V. Uivarosi, N. Mitrea, C. M. Dragoi and A. Nicolae, *Biopolym. Cell*, 2011, **27**, 141–146.
50 H. Sun, H. Li and P. J. Sadler, *Chem. Rev.*, 1999, **99**, 2817–2842.
51 A. D. Tinoco and A. M. Valentine, *J. Am. Chem. Soc.*, 2005, **127**, 11218–11219.
52 M. C. Cox, K. J. Barnham, T. A. Frenkiel, J. D. Hoeschele, A. B. Mason, Q. Y. He, R. C. Woodworth and P. J. Sadler, *JBIC, J. Biol. Inorg. Chem.*, 1999, **4**, 621–631.
53 C. D. Quarles Jr., J. L. Brumaghim and R. K. Marcus, *Metallomics*, 2010, **2**, 154–161.
54 J. B. Vincent and S. Love, *Biochim. Biophys. Acta, Gen. Subj.*, 2012, **1820**, 362–378.
55 J. Toneatto, P. F. Garcia and G. A. Argüello, *J. Inorg. Biochem.*, 2011, **105**, 1299–1305.
56 P. F. Garcia, J. Toneatto, M. J. Silvero and G. A. Argüello, *Biochim. Biophys. Acta, Gen. Subj.*, 2014, **1840**, 2695–2701.
57 W. Guo, W. Zheng, Q. Luo, X. Li, Y. Zhao, S. Xiong and F. Wang, *Inorg. Chem.*, 2013, **52**, 5328–5338.
58 L. Messori, F. G. Vilchez, R. Vilaplana, F. Piccioli, E. Alessio and B. Keppler, *Met. – Based Drugs*, 2000, **7**, 335–342.
59 F. Piccioli, S. Sabatini, L. Messori, P. Orioli, C. G. Hartinger and B. K. Keppler, *J. Inorg. Biochem.*, 2004, **98**, 1135–1142.
60 R. K. Koiri, A. Mehrotra and S. K. Trigun, *Med. Hypotheses*, 2013, **80**, 841–846.
61 F. Kratz and L. Messori, *J. Inorg. Biochem.*, 1993, **49**, 79–82.
62 F. Li, M. Feterl, J. M. Warner, A. I. Day, F. R. Keene and J. G. Collins, *Dalton Trans.*, 2013, **42**, 8868.
63 F. Kratz, M. Hartmann, B. Keppler and L. Messori, *J. Biol. Chem.*, 1994, **269**, 2581–2588.
64 L. Messori, G. Dal Poggetto, R. Monnanni and J. Hirose, *BioMetals*, 1997, **10**, 303–313.
65 O. Mazuryk, K. Kurpiewska, K. Lewiński, G. Stochel and M. Brindell, *J. Inorg. Biochem.*, 2012, **116**, 11–18.
66 D. M. Martin, N. D. Chasteen and J. K. Grady, *Biochim. Biophys. Acta*, 1991, **1076**, 252–258.
67 S. M. Page, S. R. Boss and P. D. Barker, *Future Med. Chem.*, 2009, **1**, 541–559.
68 M. Pongratz, P. Schluga, M. A. Jakupec, V. B. Arion, C. G. Hartinger, G. Allmaier and B. K. Keppler, *J. Anal. At. Spectrom.*, 2004, **19**, 46.
69 A. Bergamo, L. Messori, F. Piccioli, M. Cocchietto and G. Sava, *Invest. New Drugs*, 2003, **21**, 401–411.
70 Z. Zhao, Z. Luo, Q. Wu, W. Zheng, Y. Feng and T. Chen, *Dalton Trans.*, 2014, **43**, 17017–17028.
71 M. Shopova and T. Gantchev, *J. Photochem. Photobiol., B*, 1990, **6**, 49–59.
72 Z. Zhang, S. Hao, H. Zhu and W. Wang, *J. Photochem. Photobiol., B*, 2008, **92**, 77–82.
73 J. Ueda, K. Takeshita, S. Matsumoto, K. Yazaki, M. Kawaguchi and T. Ozawa, *Photochem. Photobiol.*, 2007, **77**, 165–170.
74 J. B. Aitken, S. Antony, C. M. Weekley, B. Lai, L. Spiccia and H. H. Harris, *Metallomics*, 2012, **4**, 1051.
75 Y. Zhang, Y. Guo, B. Wu, H. Zhang, C. Liu, J. Ma, Y. Dai, R. Xu and Z. Yang, *Biotechnol. Lett.*, 2013, **35**, 1997–2004.
76 T. R. Daniels, E. Ortiz-Sánchez, R. Luria-Pérez, R. Quintero, G. Helguera, B. Bonavida, O. Martínez-Maza and M. L. Penichet, *J. Immunother.*, 2011, **34**, 500–508.
77 T. R. Daniels-Wells, G. Helguera, J. A. Rodríguez, L. S. Leoh, M. A. Erb, G. Diamante, D. Casero, M. Pellegrini, O. Martínez-Maza and M. L. Penichet, *Toxicol. In Vitro*, 2013, **27**, 220–231.
78 J. W. Dobrucki, *J. Photochem. Photobiol. B.*, 2001, **65**, 136–144.
79 A. Martincic, R. Milacic, J. Vidmar, *et al.*, *J Chromatography A*, 2014, **1371**, 168–176.